KRONOS FUSION ENERGY

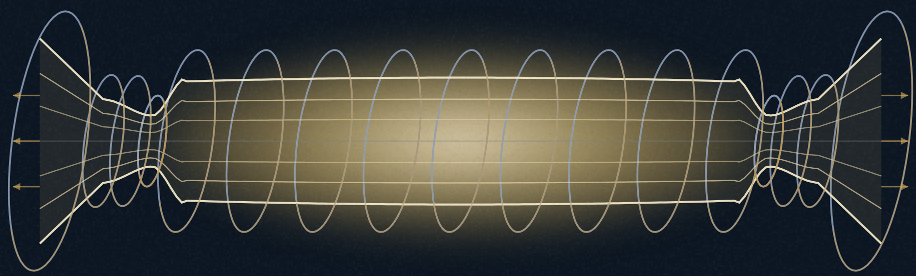

PAPER 2.26 · THE KRONOS 2026 SERIES

The Centrepost Life-Limiter: Fast-Fluence, dpa, and Shielding Setting the Cartridge-Replacement Cadence for a Compact Spherical-Tokamak Breeder

The inboard centrepost is the defining vulnerability of a normal-conductor spherical tokamak: it sits closest to the fusion source and cannot be thickly shielded without growing...

Read it live — 3-D model · physics validator · film series

BY P I FORD, R J WEGGEL AND C WEGGEL

2026 · EDITORIAL EDITION

THE OFFICIAL RECORD

What this document is, and how to read its numbers

This is a combined editorial. It gathers, in one volume, the two design studies Kronos Fusion Energy released in 2026 — a compact spherical-tokamak tritium/helium-3 breeder and a deuterium–helium-3 tandem-mirror generator — together with the intellectual-property estate, the people, and, in the internal edition, the full commercial case. The scientific text is the same text that appears in the arXiv preprints and the journal submissions; the editorial adds the apparatus a reader needs to hold the whole program at once, and nothing in the physics is altered to fit it.

THE HONESTY STANCE IS THE ASSET

Every headline quantity carries an **evidence class** — DERIVED RECOMPUTED MEASURED REQUIREMENT — and, where a number is a modelled extrapolation rather than a demonstrated value, it is labelled as such and its downside is shown next to it. Several quantities in the underlying corpus moved after first publication; where a value has been withdrawn or restated, the record says so plainly. This is deliberate: a diligence team will find the load-bearing assumptions, so the document surfaces them first.

TWO EDITIONS

This volume is issued in two editions. The **public edition** (light) carries the physics and the design only — no dollar, price, or per-kilogram figure appears anywhere in it. The **internal edition** (dark) adds the economics, the funding architecture, and the defense-commercial analysis, and is marked *Confidential* accordingly; it is not for public distribution. Where the commercial case rests on a modelled assumption rather than a demonstrated one, it is labelled as such and its downside is shown alongside it, on the same terms as the physics.

TITLE	The Kronos Fleet — Hyperion · Aegis · MetroVolt: A Combined Design & Commercialization Study
AUTHOR	Priyanca Ford, Founder & CEO, on behalf of Kronos Fusion Energy
EDITION	2026 Combined Editorial · first issue
COMPANION WORKS	The five-paper arXiv drop — (1) Breeder, (2) Burner, (3) REBCO magnet & tape, (4) Direct Energy Conversion, (5) AI/ML/Quantum control — with matching numbered Zenodo deposits, plus the IOP journal and IAEA-FEC submissions. Patents were filed before the drop.
NAMING	Hyperion = the breeder; Aegis (defense) and MetroVolt (data-center) = one generator in two housings. Internal mode letters (D1, L) do not appear on public surfaces.
STATUS	Conceptual design & simulation study. Nothing herein is a construction commitment.

HOW TO READ THIS VOLUME

The fleet at a glance, and the way its numbers are marked

This volume opens with *Orientation*, presents the five research papers as a bound sequence, and closes with the *Apparatus*. *Foundations* sets out the three general results both machines rest on. *Paper One* is the Hyperion breeder; *Paper Two* the Aegis / MetroVolt generator; *Papers Three, Four and Five* are the enabling science — high-field REBCO magnets and tape, direct energy conversion, and the AI / ML / quantum control stack. A *Digital Twin & 3-D Model* part follows, then the *Environmental* profile. The *Economics* and levelized cost and the *Business Case* and diligence record appear in the internal edition only; the *Simulations* proof record and the Apparatus — patent portfolio, team, limitations, and sources — close both editions.

THE FLEET AT A GLANCE

	HYPERION	AEGIS	METROVOLT
Role	Strategic-isotope foundry	Defense installation power	Campus power
Machine	**Spherical tokamak**	**Tandem mirror**	**Tandem mirror**
Fuel	Deuterium–tritium	Deuterium–helium-3	Deuterium–helium-3
Delivers	Tritium · ^{3}He · 14 MeV n	Resilient installation power	Firm campus power
Physics bar	**Fusion gain only**	Closure (gates named)	Closure + lunar ^{3}He
In the fleet	Breeds the fuel	Proves the generator	Commercial destination

HOW THE NUMBERS ARE MARKED

Every headline quantity carries an evidence class — DERIVED from first principles, RECOMPUTED from raw data, MEASURED in hardware, or a REQUIREMENT yet to be met. Financial figures carry a case label and are confined to the internal (confidential) edition. Values that moved after first publication are shown as withdrawn or restated rather than quietly changed. A capability you can evaluate is one whose limits are on the page.

ABSTRACT

The Centrepost Life-Limiter: Fast-Fluence, dpa, and Shielding Setting the Cartridge-Replacement Cadence for a Compact Spherical-Tokamak Breeder

The inboard centrepost is the defining vulnerability of a normal-conductor spherical tokamak: it sits closest to the $14.06\,MeV$ fusion source and cannot be thickly shielded without growing the machine or displacing the breeding blanket. We do not argue this away; we quantify it and design for it. We solve the steady linear Boltzmann transport equation for the Hyperion breeder ($R_0 = 1.20\,m$, aspect ratio $A = 2.5$, $B_0 = 8\,T$, $I_p = 9.66\,MA$, $P_{\text{fus}} = 85.04\,MW$, negative triangularity $\delta = -0.30$, elongation $\kappa = 2.0$, centrepost peak field $16.84\,T$) with Monte-Carlo neutron transport on ENDF/B-VIII.0, scoring the fast-neutron fluence ($E > 0.1\,MeV$) and the displacement damage at the centrepost REBCO tape behind a tungsten-carbide (WC) shield of variable thickness, and we fold the tallied spectrum against a Norgett–Robinson–Torrens (NRT) damage function corrected by an athermal-recombination (arc-dpa) efficiency. A $45\,cm$ inboard standoff attenuates the centrepost fast fluence by a factor of 169, from $2.93e25$ $\mathrm{n\,m^{-2}\,fpy^{-1}}$ bare to $1.73e23$ $\mathrm{n\,m^{-2}\,fpy^{-1}}$ at full WC, with an effective removal coefficient that hardens from $0.070\,/cm$ near the source to $0.141\,/cm$ in the clean deep spectrum. At the design shield the reference structural damage rate is 18.85 $\mathrm{fpy^{-1}}$ and, at the REBCO fast-fluence damage ceiling $\Phi_{\text{allow}} \approx 3.9e22\,\mathrm{n\,m^{-2}}$, the cartridge life is 0.22 fpy; a thin $5\,cm$ shield gives 0.0048 fpy and a thick $40\,cm$ shield 0.194 fpy, so shielding trades directly and monotonically against inboard breeding coverage (net 1-D TBR falls from 1.035 to 0.923). The centrepost-life ceiling caps the admissible plasma current to $[8.78\,,9.66\,]\,\mathrm{MA}$; the mid-current point extends life to 0.496 fpy ($\times 2.25$). The design consequence is a maintenance architecture — a demountable, scheduled-swap cartridge at ~ 4.5–$4.9\,\mathrm{swaps\,fpy^{-1}}$ — not a materials miracle. Every headline quantity is a frozen anchor in the Kronos de-risking register.

Open-access deposit (code & data, CC BY 4.0): DOI 10.5281/zenodo.22645708 · Zenodo community *kronos_fusion_energy*. Explore it live: interactive 3-D model · physics validator.

Keywords: centrepost · fast neutron fluence · displacement damage · dpa · tungsten-carbide shield · REBCO coated conductor · scheduled-replacement cartridge · spherical-tokamak breeder

CONTENTS

Table of Contents

The Centrepost Life-Limiter: Fast-Fluence, dpa, and Shielding Setting the Cartridge-Replacement Cadence for a Compact Spherical-Tokamak Breeder 3
Introduction 6
Governing equations and the formal problem 7
Computational methodology: the GPU-HPC campaign 10
Results 13
Discussion 21
Limitations 22
Conclusion 23
References 28
One programme, many papers 31

NOMENCLATURE

Symbols, units, and the names of things

Q	plasma (fusion) gain, P_{fus}/P_{aux}
Q_E	engineering gain, net electric out / recirculating in
H_{98}	confinement enhancement over the IPB98(y,2) scaling
Z_{eff}	effective ion charge
c_{ee}	electron–electron bremsstrahlung leading coefficient, 2.120022 (exact)
τ_E	energy confinement time
I_p	plasma current
R_0, a	major radius, minor radius
κ, δ	elongation, triangularity
β_N	normalized plasma beta (Troyon-normalized)
TBR	tritium breeding ratio
DEC	direct energy conversion
CF	plant capacity factor (availability)
FOAK / NOAK / BOAK	first / n^{th} / best of a kind
Hyperion	the ST breeder (internal: Mode D2)
Aegis	the generator, defense/installation housing (internal: Mode M)
MetroVolt	the generator, data-center housing (Mode M)

§ 1

Introduction

THE CENTREPOST PROBLEM

A spherical tokamak (ST) confines a large plasma current in a small volume, which is exactly what makes it an efficient $14\,MeV$ neutron source and tritium breeder [1,2], and, at the same time, what forces its hardest engineering compromise. To reach aspect ratio $A = 2.5$ at major radius $R_0 = 1.20\,m$ the inboard toroidal-field return — the *centrepost* — must be slender, and it therefore sits only tens of centimetres from the plasma with almost no room for shielding. Every high-field ST power-plant study confronts the same fact: the centrepost is the most neutron-exposed structural and magnetic element in the machine, and no shield that fits inside the geometry can protect it to a multi-decade life. This is the price of compactness, and it is best paid openly.

The response taken here follows the demountable-magnet philosophy of ARC [3] to its logical conclusion: rather than claiming a lifetime centrepost, we treat it as a *consumable, scheduled-replacement cartridge* and design the machine for its periodic removal. The engineering question then changes from an intractable materials problem ("how do we make a magnet survive $10^{27}\,\mathrm{n\,m^{-2}}$?") to a tractable maintenance-interval problem ("how often must the cartridge be swapped, and can the plant tolerate that cadence?"). Answering it requires three quantities computed to nuclear-data fidelity: the fast-neutron fluence at the conductor, the displacement damage in the surrounding structure, and the way both scale with an inboard shield that is itself in competition with the breeding blanket. This paper computes all three, and converts them into a replacement cadence.

PRIOR ART

The neutron shielding of superconducting cores in compact tokamaks has an established literature. Windsor and co-workers mapped the neutron and gamma flux through tungsten- and tungsten-boride-based shields protecting the superconducting centre column of an ST power plant, and quantified the heat deposition and damage that a practical shield must suppress [7,8,9]. The ARC line established the compact high-field, demountable-magnet reactor concept and the associated inboard-build pressure [3,4]. Systems codes such as PROCESS carry parametric centrepost and shield models across the ST design space [5,6]. On the materials side, the displacement-damage framework rests on the Norgett–Robinson–Torrens (NRT) standard [10], its Kinchin–Pease [11] and Lindhard [12] antecedents, and the modern athermal-recombination (arc-dpa) correction of Nordlund *et al.* [13,14] with effective threshold and efficiency evaluations by Konobeyev *et al.* [15]; the fusion-materials context is set by Zinkle [23,24], Gilbert [25], Stork [26] and the DEMO programme [27]. The specific vulnerability of REBCO coated conductors to fast-neutron irradiation — a critical-current degradation onset in the 10^{22}–$10^{23}\,\mathrm{n\,m^{-2}}$ range — has been measured by Fischer, Prokopec, Eisterer and co-workers [19,20] and underpins the high-field no-insulation (NI) REBCO magnets that make the compact ST possible [21,22].

CONTRIBUTION

What the prior art leaves open for a *breeder* is the coupled ledger: the same $45\,cm$ of inboard radius is contested between the shield that buys centrepost life and the mantle that breeds tritium, and the correct design point is the one that respects both. This paper contributes (i) a formal statement of the transport-and-damage problem with the attenuation, NRT/arc-dpa and damage-limited-life functionals written explicitly (§2); (ii) a high-statistics Monte-Carlo solution on ENDF/B-VIII.0 that resolves the centrepost fast-fluence attenuation to sub-percent tally error and extracts a depth-dependent removal coefficient (§3–4); (iii) the coverage-versus-protection optimisation cast as a constrained program whose Karush–Kuhn–Tucker (KKT) solution is the observed corner design (full WC standoff, outboard breeding); (iv) the map from damage ceiling to cartridge life to replacement cadence and fleet availability; and (v) the current-window coupling that ties the centrepost-life ceiling to the admissible plasma current. Every number traces to a frozen serial in the Kronos Physics De-Risking Register [33], cited inline (e.g.\ BR-L1-A13b). The result sits within a companion set: the consumable-centrepost neutronics and coil-integrity overview [34], the first-principles REBCO radiation-tolerance study that fixes the fluence ceiling [35], the operating-window synthesis [36], the tritium-breeding fleet case [37], the first-wall damage-and-lifetime study [38], the prognostics and remaining-useful-life framework [39], and the swap-logistics and fleet-RAMI analyses [40,41] that consume the cadence derived here.

§ 2

Governing equations and the formal problem

NEUTRON TRANSPORT

The centrepost fluence is the solution of the steady-state, fixed-source linear Boltzmann transport equation for the angular neutron flux $\psi(\mathbf{r}, \boldsymbol{\Omega}, E)$,

$$\boldsymbol{\Omega}\cdot\nabla\psi + \Sigma_t(\mathbf{r}, E)\,\psi = \int_0^\infty \mathrm{d}E' \oint_{4\pi} \mathrm{d}\boldsymbol{\Omega}'\,\Sigma_s(\mathbf{r}, E'\to E, \boldsymbol{\Omega}'\cdot\boldsymbol{\Omega})\,\psi(\mathbf{r}, \boldsymbol{\Omega}', E') + \frac{S(\mathbf{r}, E)}{4\pi},$$

with Σ_t and Σ_s the macroscopic total and differential-scattering cross-sections from ENDF/B-VIII.0, and S the fusion source. For a D–T plasma the source is a near-monoenergetic $14.06\,MeV$ emission,

[redacted]

where χ_{DT} is the Gaussian-broadened D–T line and f_{src} its spatial distribution (a toroidal ring at R_0). The scalar flux is $\phi(\mathbf{r}, E) = \oint_{4\pi} \psi\,\mathrm{d}\boldsymbol{\Omega}$, and the neutron wall loading that anchors the reference damage rate is $\Gamma_w = 1.885\,MW/m^2$ (serial BR-L1-A13).

THE FAST-FLUENCE FUNCTIONAL AND THE ATTENUATION MODEL

The quantity that limits the REBCO conductor is the accumulated fast fluence above the damage threshold $E_c = 0.1\,MeV$ at the peak-tape monitor cell $\mathbf{r}_{\mathrm{cp}}$,

$$\dot{\Phi}_{\mathrm{fast}}(\mathbf{r}_{\mathrm{cp}}) = \int_{E_c}^{\infty} \phi(\mathbf{r}_{\mathrm{cp}}, E)\,\mathrm{d}E, \qquad \Phi_{\mathrm{fast}}(t) = \int_0^t \dot{\Phi}_{\mathrm{fast}}\,\mathrm{d}t',$$

reported per full-power year (fpy). Along the inboard radius the transmitted fast fluence through a shield of thickness x obeys the classical removal-plus-buildup form

$$\dot{\Phi}_{\mathrm{fast}}(x) = \dot{\Phi}_0\,B(x)\,\exp\Big[-\int_0^x \Sigma_r(x')\,\mathrm{d}x'\Big],$$

with Σ_r the macroscopic removal cross-section for fast neutrons in the shield material and $B(x) \geq 1$ the buildup factor accounting for in-scattered neutrons that re-enter the fast group. Equation (4) defines an *effective* depth-dependent removal coefficient,

$$\Sigma_r^{\mathrm{eff}}(x) \equiv -\frac{\mathrm{d}}{\mathrm{d}x}\ln\dot{\Phi}_{\mathrm{fast}}(x),$$

which we extract directly from the Monte-Carlo tally (§4) and which rises with depth as the buildup of degraded neutrons is progressively removed and the surviving spectrum hardens toward the clean 14.06-MeV attenuation length.

THE DISPLACEMENT-DAMAGE FUNCTIONAL

The structural damage that governs the steel liner, first wall and centrepost jacket is the displacement rate. A neutron of energy E transfers recoil energy T to a lattice atom with cross-section $\mathrm{d}\sigma/\mathrm{d}T$; only the nuclear-stopping part of T produces displacements, given by the Lindhard partition

$$T_{\mathrm{dam}}(T) = \frac{T}{1 + k\,g(\varepsilon)}, \qquad g(\varepsilon) = 3.4008\,\varepsilon^{1/6} + 0.40244\,\varepsilon^{3/4} + \varepsilon,$$

with ε the reduced recoil energy and k the Lindhard electronic-stopping constant. The Norgett–Robinson–Torrens number of stable Frenkel pairs per primary knock-on atom (PKA) is [10]

$$\nu_{\mathrm{NRT}}(T_{\mathrm{dam}}) = \begin{cases} 0, & T_{\mathrm{dam}} < E_d, \\ 1, & E_d \le T_{\mathrm{dam}} < \dfrac{2E_d}{0.8}, \\ \dfrac{0.8\,T_{\mathrm{dam}}}{2E_d}, & T_{\mathrm{dam}} \ge \dfrac{2E_d}{0.8}, \end{cases}$$

with E_d the effective threshold displacement energy. The NRT displacement rate then folds the flux against the damage cross-section,

$$R_{\mathrm{dpa}}^{\mathrm{NRT}} = \frac{0.8}{2E_d}\int_0^\infty \phi(E)\left[\int_{E_d}^{T_{\max}(E)} \frac{\mathrm{d}\sigma}{\mathrm{d}T}\,T_{\mathrm{dam}}(T)\,\mathrm{d}T\right]\mathrm{d}E \;\equiv\; \int_0^\infty \phi(E)\,\sigma_D(E)\,\mathrm{d}E,$$

where $\sigma_D(E)$ is the NJOY-processed damage-energy cross-section (reaction MT$=444$). Molecular-dynamics cascade evidence shows the NRT number overestimates surviving damage because of athermal in-cascade recombination; the arc-dpa model [13,14] multiplies ν_{NRT} by an efficiency

$$\xi_{\mathrm{arc}}(T_{\mathrm{dam}}) = \frac{1-c_{\mathrm{arc}}}{(2E_d/0.8)^{b_{\mathrm{arc}}}}\,T_{\mathrm{dam}}^{b_{\mathrm{arc}}} + c_{\mathrm{arc}}, \qquad \xi_{\mathrm{arc}} \to c_{\mathrm{arc}} \approx 0.3 \text{ as } T_{\mathrm{dam}} \to \infty,$$

so that at the $\mathcal{O}(10\text{--}30\ \mathrm{keV})$ cascade energies characteristic of 14-MeV recoils in Fe and W (serial BR-L2-A24) the surviving-damage rate is $R_{\mathrm{dpa}}^{\mathrm{arc}} \approx 0.3\,R_{\mathrm{dpa}}^{\mathrm{NRT}}$. We report the register anchor 18.85 fpy^{-1} on the NRT convention (BR-L1-A13; wall-loading-anchored value 19.66 fpy^{-1}, BR-SX-02) and carry the arc-dpa efficiency as the conservatism margin.

DAMAGE-LIMITED CARTRIDGE LIFE

The centrepost is retired when its accumulated fast fluence reaches the REBCO critical-current-degradation ceiling Φ_{allow}. The cartridge life and replacement cadence are therefore

$$T_c(x) = \frac{\Phi_{\mathrm{allow}}}{\dot{\Phi}_{\mathrm{fast}}(x)}, \qquad n_{\mathrm{swap}}(x) = \frac{1}{T_c(x)} = \frac{\dot{\Phi}_{\mathrm{fast}}(x)}{\Phi_{\mathrm{allow}}},$$

in fpy and swaps fpy^{-1} respectively. The ceiling is not a free parameter: first-principles DFT+U chain-oxygen-vacancy formation and YBCO displacement-cascade molecular dynamics place the onset at [redacted] for artificial-pinning-centre tape (un-doped break-even [redacted]; serials BR-SX-04 and companion [35]). We bracket the sensitivity with the commonly cited 1×10^{22} (conservative) and $1\times10^{23}\,\mathrm{n\,m^{-2}}$ (optimistic) limits.

COVERAGE VERSUS PROTECTION AS A CONSTRAINED PROGRAM

The inboard standoff of fixed thickness $L = 45\,cm$ is partitioned between a WC shield of thickness x (inner, protecting the conductor) and a lithium breeding mantle of thickness $L - x$ (outer, breeding tritium). Both the cartridge life and the net tritium-breeding ratio $\Lambda(x)$ depend on x, and they pull in opposite directions: thicker WC raises T_c but starves the inboard mantle. The design point solves

$$x^\star = \arg\max_{0\le x\le L}\; T_c(x) \quad \text{s.t.} \quad \Lambda(x) \ge \Lambda_{\min},$$

with Lagrangian $\mathcal{L}(x,\mu) = T_c(x) + \mu\,[\Lambda(x) - \Lambda_{\min}]$ and stationarity

$$\frac{\mathrm{d}T_c}{\mathrm{d}x} + \mu\,\frac{\mathrm{d}\Lambda}{\mathrm{d}x} = 0, \qquad \mu\,[\Lambda(x) - \Lambda_{\min}] = 0, \qquad \mu \ge 0.$$

Because $T_c'(x) > 0$ and $\Lambda'(x) < 0$ everywhere on $[0, L]$ (§4), an interior optimum would require $\mu > 0$ with the breeding constraint active. The 1-D radial calculation, however, returns $\Lambda(x) < 1$ for *all* x (the inboard side cannot reach self-sufficiency), so the constraint $\Lambda(x) \ge \Lambda_{\min}$ with a self-sufficient $\Lambda_{\min}$ is infeasible inboard and the breeding target is instead met from the outboard blanket and multiplier (companions [37,36]). With the inboard breeding requirement relaxed, (12) has its maximiser at the corner $x^\star = L$: the full standoff is given to WC, and the inboard mantle breeds nothing. This corner solution is exactly the register's recommended operating shield (BR-L1-A13b).

CURRENT-WINDOW COUPLING

Because $\dot{\Phi}_{\text{fast}} \propto S_n \propto P_{\text{fus}}$ and $R_{\text{dpa}} \propto S_n$, the centrepost-life ceiling is equivalent to a fusion-power ceiling and, through the confinement scaling, to a plasma-current ceiling. Writing the damage constraint $R_{\text{dpa}}(I_p) \leq R_{\text{dpa}}^{\text{max}} = 18.85$ fpy^{-1} and the life floor $T_c(I_p) \geq T_c^{\text{min}}$, the admissible current window is (serial KX-L1-A21)

$$I_p \in [\,8.78\,\text{MA},\ 9.66\,\text{MA}\,],$$

over $q_{95} \in [2.7, 3.3]$, with the tritium-startup floor non-binding. Reducing the operating point from the design current to the mid-current edge of (13) lowers the source strength and extends the cartridge life by the register factor $T_c^{\text{mid}}/T_c^{\text{des}} = 0.496/0.22 = 2.25$ (serial BR-SX-16).

§ 3

Computational methodology: the GPU-HPC campaign

MONTE-CARLO TRANSPORT

Equation (1) is solved by the open-source Monte-Carlo code OpenMC 0.15.3 [16] on the ENDF/B-VIII.0 continuous-energy library [17] (endfb80-lowtemp HDF5), continuous-energy and temperature-corrected. The frozen design point is transported in a one-dimensional radial infinite-cylinder constructive-solid-geometry (CSG) model: concentric z-cylinders about the machine axis with reflective z-planes (no axial leakage, clean radial transport), and a $14.06\,MeV$ isotropic ring source at $R_0 = 120\,cm$ uniform in azimuth and height (figures 1–2). The inboard radial build, from the axis outward, is: centrepost magnet bundle $r = 0–21.6\,cm$ (homogenised Cu 60 vol%+ SS316 40 vol% "REBCO_centrepost" proxy); the REBCO peak-tape monitor cell $r = 21.6\,–23.6\,cm$ (the fluence-tally location); a fixed $45\,cm$ tradeable standoff $r = 23.6\,–68.6\,cm$ split as WC shield (inner) plus lithium breeding mantle (outer); then the steel liner and tungsten first wall; then the plasma. The trade knob is the shield thickness $x = 45 - t_{\text{mantle}}$ for $t_{\text{mantle}} \in \{0, 15, 30, 45\}$ cm (serial BR-L1-A13b).

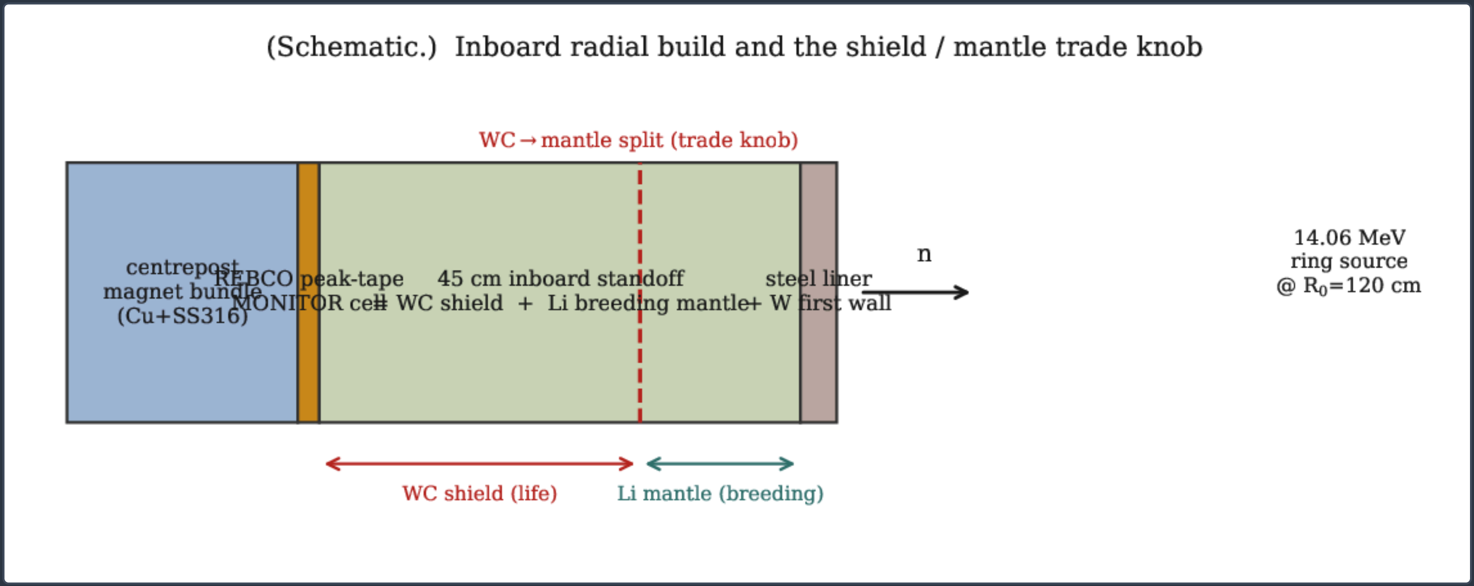

(Schematic.) Inboard radial build transported in the OpenMC model, from the machine axis outward: centrepost magnet bundle, REBCO peak-tape fluence-monitor cell, the $45\,cm$ tradeable standoff split between WC shield (protection) and lithium breeding mantle (coverage), and the steel liner / tungsten first wall. The red dashed line is the shield→mantle trade knob of the constrained program (11). No data values are shown.

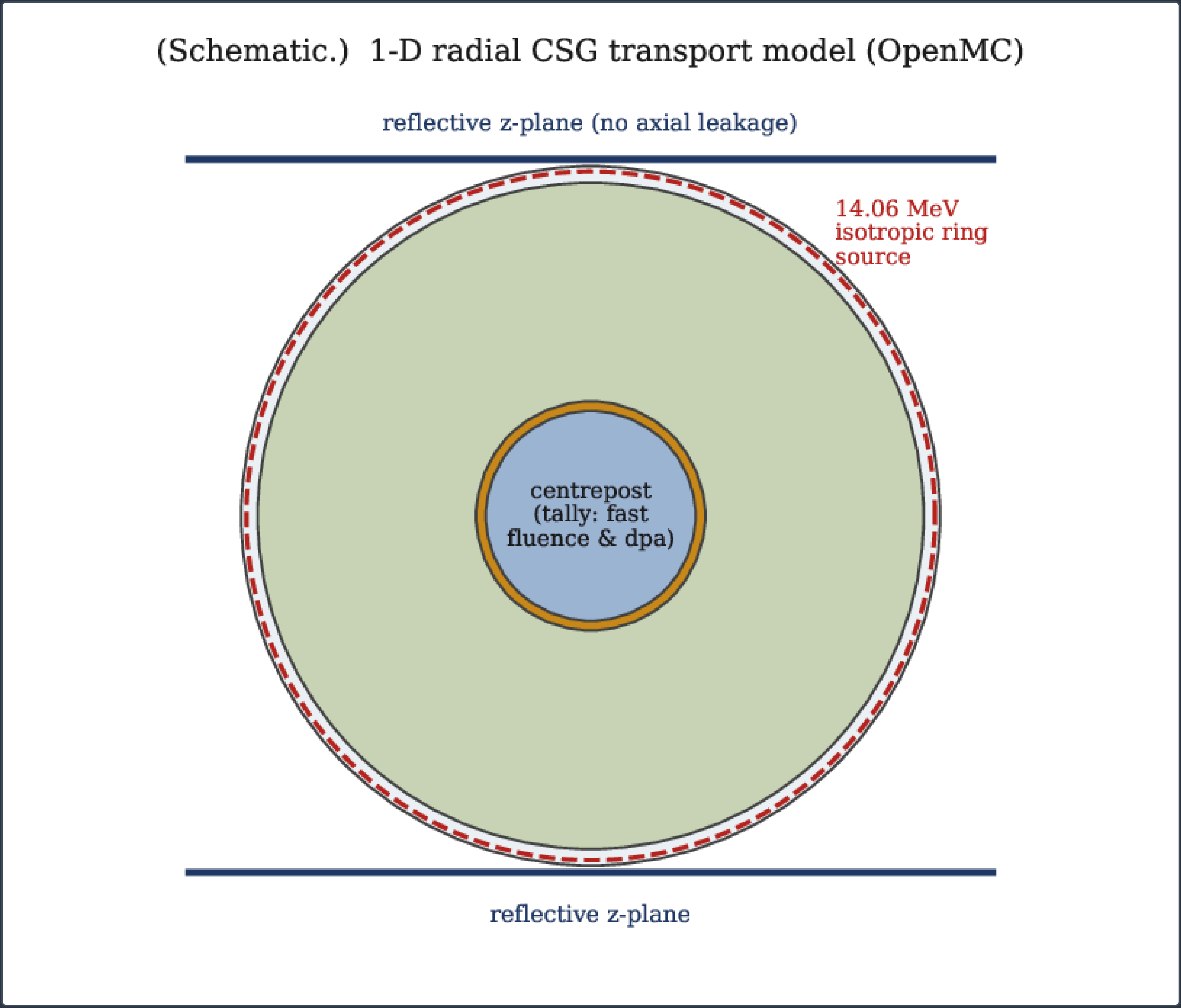

(Schematic.) The 1-D radial infinite-cylinder CSG transport model: concentric z-cylinders about the machine axis with reflective z-planes (no axial leakage) and a $14.06\,MeV$ isotropic ring source at $R_0 = 120\,cm$. The fast fluence and displacement damage are tallied at the centrepost monitor cell. The figure encodes structure only.

DAMAGE CROSS-SECTIONS AND MULTISCALE PKA MODELLING

The damage-energy cross-section $\sigma_D(E)$ of equation (8) is generated with the NJOY nuclear-data processing system [18] (HEATR module, MT$=444$) from the same ENDF/B-VIII.0 evaluations, and the NRT number of equation (7) is applied group-wise. To justify the arc-dpa efficiency of equation (9) at the cascade level, primary-knock-on spectra are computed with SPECTRA-PKA driven by the NJOY21 recoil matrices and propagated into molecular-dynamics displacement cascades in LAMMPS: 15-keV Fe–9Cr and tungsten cascades are run and analysed for surviving Frenkel pairs by Wigner–Seitz occupancy (serial BR-L2-A24), with effective threshold and arc-dpa parameters cross-checked against the evaluations of Konobeyev, Fischer and Simakov [15,14] and the multiscale radiation-damage chain of serial HX-20. The REBCO fast-fluence ceiling is set independently by DFT+U chain-oxygen-vacancy formation energies and YBCO displacement-cascade MD (companion [35]; serial BR-SX-04).

SCALE, ACCELERATION AND REPRODUCIBILITY

Each of the four shield-split points was run at 5×10^7 particles per batch over 50 active batches, for 2.5×10^9 neutron histories per point, on the NVIDIA GPU HPC campaign (Lambda A100/H100/A10 fleet); the Monte-Carlo history transport and the batch-parallel tally reduction map onto the GPU fleet, while the NJOY processing, the LAMMPS cascade analysis and the trade-curve reduction run on the in-house HPC node so the two workloads never contend. The variance is small and machine-checkable: the net-TBR relative error is $\sim 2 \times 10^{-5}$ and the centrepost fast-flux relative error is 0.02–0.24% across the split points (table 3). The transport model, source normalisation of equation (2), radial build and tally definitions are archived byte-for-byte and are regenerable from the cited serials; no result depends on proprietary data. Table 1 collects the codes, library, problem scale and verification metrics.

ELEMENT	SPECIFICATION	ROLE
transport code	OpenMC 0.15.3 [16]	fixed-source neutron transport, eq. (1)
nuclear data	ENDF/B-VIII.0 [17]	continuous-energy cross-sections
damage processing	NJOY (HEATR, MT$=444$) [18]	damage-energy $\sigma_D(E)$, eq. (8)
PKA / cascade	SPECTRA-PKA + NJOY21 $\rightarrow$ LAMMPS	15-keV Fe–9Cr, W cascades (BR-L2-A24)
REBCO ceiling	DFT+U + YBCO cascade MD	Φ_{allow}, eq. (10) (BR-SX-04)
geometry	1-D radial infinite-cylinder CSG	reflective z, ring source at R_0
histories / point	$5 \times 10^7 \times 50 = 2.5 \times 10^9$	4 shield-split points (BR-L1-A13b)
hardware	NVIDIA GPU HPC campaign	A100 / H100 / A10 fleet
TBR tally error	$\sim 2 \times 10^{-5}$ (rel.)	verification
cp fast-flux error	0.02–0.24% (rel.)	verification

Computational specification and reproducibility metrics for the centrepost transport-and-damage campaign. Serials refer to the Kronos de-risking register [33]. No compute-cost figures are reported.

§ 4

Results

DESIGN POINT AND THE REFERENCE DAMAGE RATE

Table 2 lists the frozen design point transported here. At the neutron wall loading $\Gamma_w = 1.885\ MW/m^2$ the reference NRT displacement rate is 18.85 fpy^{-1} (BR-L1-A13), the ceiling that the current window of equation (13) is built to respect. This is a first-wall–referenced structural rate; the fast fluence that actually retires the centrepost conductor is the attenuated quantity computed next.

QUANTITY	SYMBOL	VALUE	
major radius	R_0	1.20 m	
aspect ratio	A	2.5	$(a = 0.48\,m)$
elongation / triangularity	κ / δ	2.0 / -0.30	negative-δ
on-axis field	B_0	8 T	
centrepost peak field	B_{cp}	16.84 T	breeder magnet
plasma current	I_p	9.66 MA	
fusion power	P_{fus}	85.04 MW	$(Q = 3.076)$
source rate	S_n	3.016e19 /s	eq. (2)
neutron wall loading	Γ_w	1.885 MW/m^2	BR-L1-A13
reference damage rate	R_{dpa}	18.85 fpy^{-1}	NRT, BR-L1-A13

Frozen Hyperion breeder design point (Tier-2 canonical anchors). Two distinct magnets are carried in the programme; this paper concerns the breeder centrepost only.

FAST-FLUENCE ATTENUATION AND THE REMOVAL COEFFICIENT

Figure 3 shows the centrepost fast fluence (equation 3) against WC shield thickness from the four high-statistics tallies. The fluence falls monotonically from $2.928e25$ $\mathrm{n\,m^{-2}\,fpy^{-1}}$ bare (full mantle, no shield) to $1.729e23$ $\mathrm{n\,m^{-2}\,fpy^{-1}}$ at full WC, a factor of 169 over the $45\,cm$ standoff. The attenuation is not a single exponential: extracting the effective removal coefficient of equation (5) interval-by-interval (figure 4) gives $\Sigma_r^{\mathrm{eff}} = 0.070\,/cm$ over 0–$15\,cm$, $0.131\,/cm$ over 15–$30\,cm$, and $0.141\,/cm$ over 30–$45\,cm$ — an e-folding length that shortens from 14.3 to $7.1\,cm$ with depth. This depth-hardening is the physical signature of buildup: near the source the fast group is continually re-populated by down-scattered 14-MeV neutrons ($B(x) \gg 1$), while deep in the shield the surviving spectrum is clean and attenuates at the material removal length. The consequence for design is that the last centimetres of shield are the most effective per unit thickness.

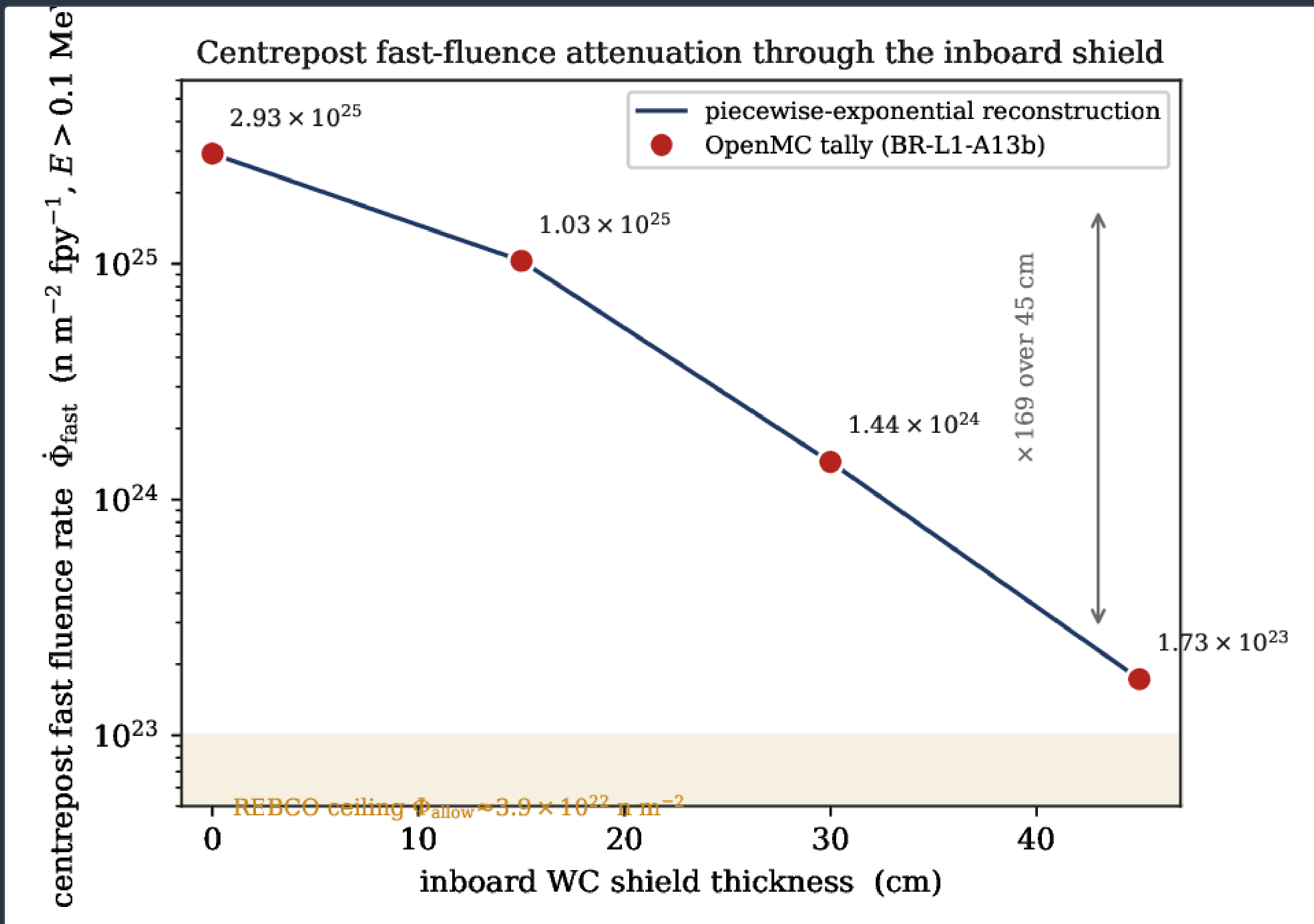

Centrepost fast-neutron fluence rate ($E > 0.1\,MeV$) versus inboard WC shield thickness, from four 2.5×10^9-history OpenMC tallies on ENDF/B-VIII.0 (serial BR-L1-A13b). The fluence falls by a factor of 169 over the $45\,cm$ standoff; the gold band marks the REBCO damage-ceiling bracket (1–$10 \times 10^{22}\,\mathrm{n\,m^{-2}}$).

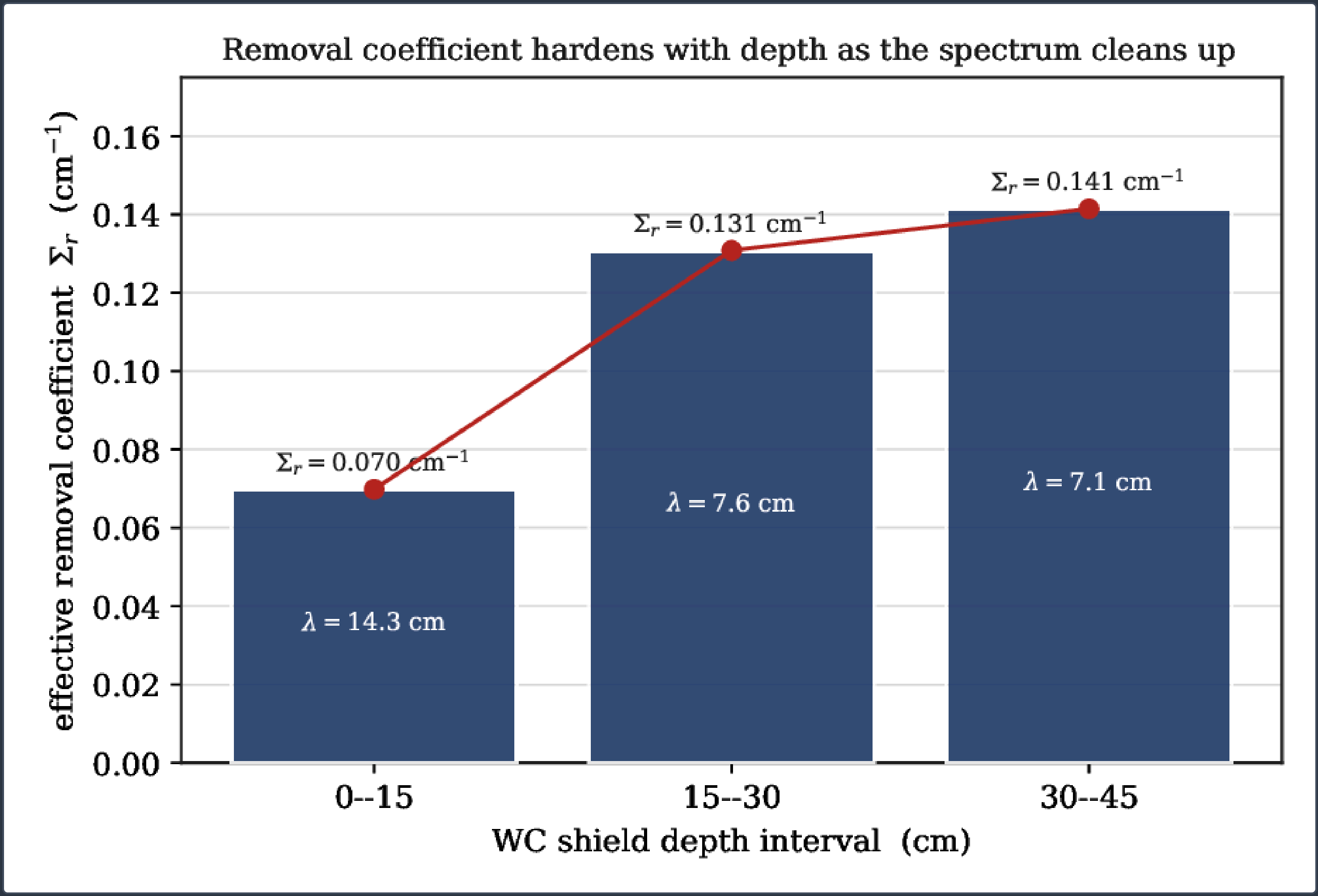

Effective removal coefficient Σ_r^{eff} (equation 5) by shield-depth interval, extracted from the tallies of figure 3. The coefficient hardens from 0.070 to 0.141 $/cm$ with depth as buildup is removed and the spectrum cleans up.

CARTRIDGE LIFE AND THE DAMAGE CEILING

Converting fast fluence to life through equation (10) requires the REBCO ceiling Φ_{allow}. Figure 5 plots the cartridge life against shield thickness at the conservative (1×10^{22}), REBCO (3.9×10^{22}) and optimistic ($1 \times 10^{23}\ \mathrm{n\,m^{-2}}$) ceilings. At the corner design (full 45 cm WC, $\dot{\Phi}_{\mathrm{fast}} = 1.729e23$ $\mathrm{n\,m^{-2}\,fpy^{-1}}$) the REBCO ceiling gives

reproducing the register design anchor of 0.22 fpy (serial SC-BR-2: 30 cm-class WC gives 0.221 fpy). Thinner shields collapse the life: 5 cm yields 0.0048 fpy and the bare centrepost only $\sim$0.003–0.004 fpy ($\sim$1.4 full-power-days, inadmissible), while a thick 40 cm shield reaches 0.194 fpy. Every candidate at any point on the standoff falls below a lifetime-component threshold by two-to-three orders of magnitude: the compact-ST centrepost *cannot* be shielded to multi-fpy life within the available inboard radius, which is precisely why it is a scheduled-replacement cartridge and not a lifetime part. Table 3 gives the full trade.

WC	LI MANTLE	$\dot{\Phi}_{fast}$	NET	T_c@10^{22}	T_c@3.9×10^{22}	T_c@10^{23}
(cm)	(cm)	($\mathrm{n\,m^{-2}fpy^{-1}}$)	TBR	(fpy)	(fpy)	(fpy)
0	45	2.928×10^{25}	1.035	0.00034	0.0013	0.0034
15	30	1.027×10^{25}	1.022	0.00097	0.0038	0.0097
30	15	1.444×10^{24}	0.997	0.0069	0.0270	0.0693
45	**0**	$\mathbf{1.729 \times 10^{23}}$	**0.923**	**0.0578**	**0.226**	**0.578**

Centrepost fast-fluence / net-TBR shield trade (serial BR-L1-A13b; OpenMC 0.15.3, ENDF/B-VIII.0, 2.5×10^9 histories/point). Life at three fast-fluence damage ceilings; the REBCO column uses $\ Phi_ allow=§I3.9e22

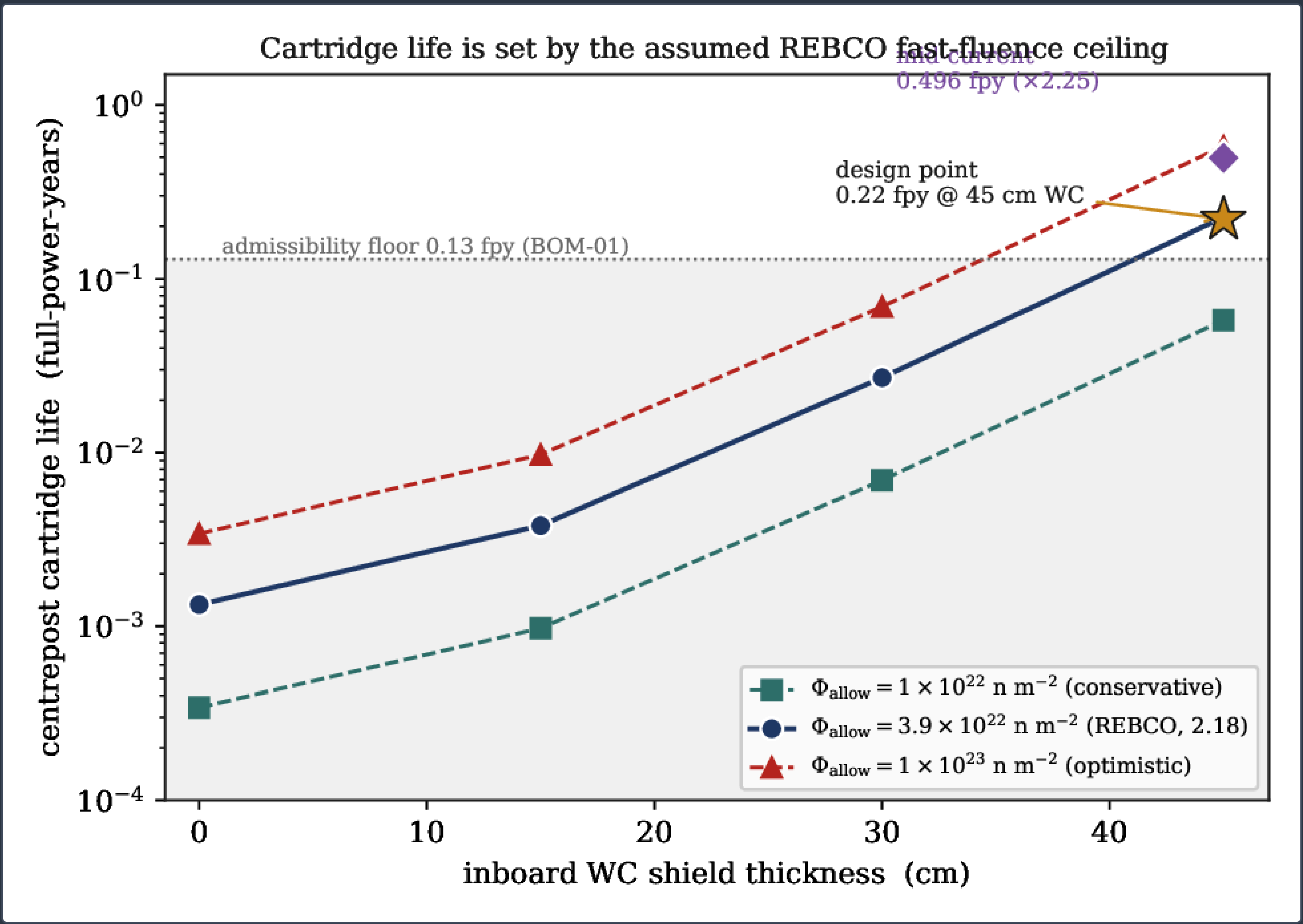

Centrepost cartridge life versus WC shield thickness at three fast-fluence damage ceilings. The design point (star) is the full 45 *cm* WC standoff at the REBCO ceiling, 0.22 fpy; the mid-current operating point extends it to 0.496 fpy. The grey band is the 0.13 fpy admissibility floor (serial BOM-01).

COVERAGE VERSUS PROTECTION

The same shield that buys centrepost life displaces the inboard breeding mantle. Figure 6 plots the net 1-D radial TBR against cartridge life as the shield–mantle split is swept, tracing the coverage-versus-protection Pareto front of the constrained program (11). Net TBR falls from **1.035** (bare) to **0.923** (full WC) while life rises by two-plus decades. Crucially the 1-D radial net TBR is below the self-sufficiency line $\Lambda_{\min} = 1.05$ at *every* split point — so, per the KKT analysis of §2.5, the inboard breeding constraint is infeasible and the optimiser sits at the corner $x^{\star} = L$: the full standoff goes to WC and tritium self-sufficiency is recovered from the outboard blanket and neutron multiplier in the 3-D closure (net TBR $\geq$ 1.05; companions [37,36]). The inboard shield is thus not a breeding surface but a protection surface, and the design accepts that trade explicitly.

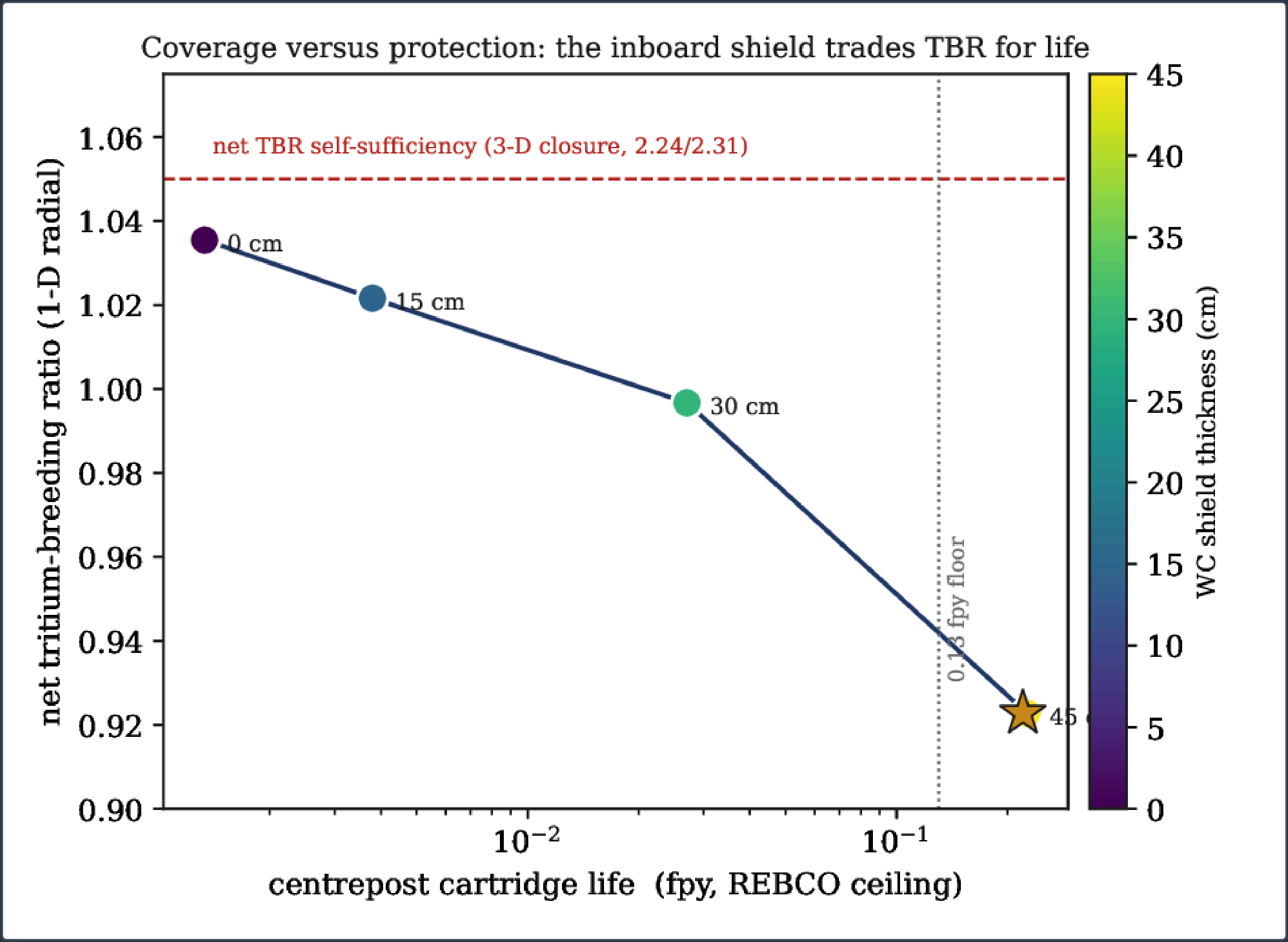

Coverage-versus-protection Pareto: net 1-D radial TBR against centrepost cartridge life (REBCO ceiling) as the WC/mantle split is swept (colour = WC thickness). Net TBR is below the **1.05** self-sufficiency line at every inboard split; self-sufficiency is met in the 3-D outboard closure. The corner design (star) gives all standoff to WC.

THE ADMISSIBLE CURRENT WINDOW

Because the fast fluence scales with source strength, the centrepost-life ceiling limits how hard the machine may be driven. Figure 7 shows the cartridge life and the displacement rate across the admissible current window of equation (13): at the design current $9.66\,MA$ the life is 0.22 fpy against the 18.85 fpy^{-1} damage ceiling, and retreating to the mid-current edge $8.78\,MA$ lowers the source strength enough to extend the life to 0.496 fpy (×2.25; serial BR-SX-16). The curve is a phenomenological interpolation anchored to the two register operating points; the strong sensitivity reflects the combined reduction of plasma current and density at the mid-current point, not a single-parameter power law. The current window is therefore the primary in-shot lever on cartridge life once the shield is fixed at the corner.

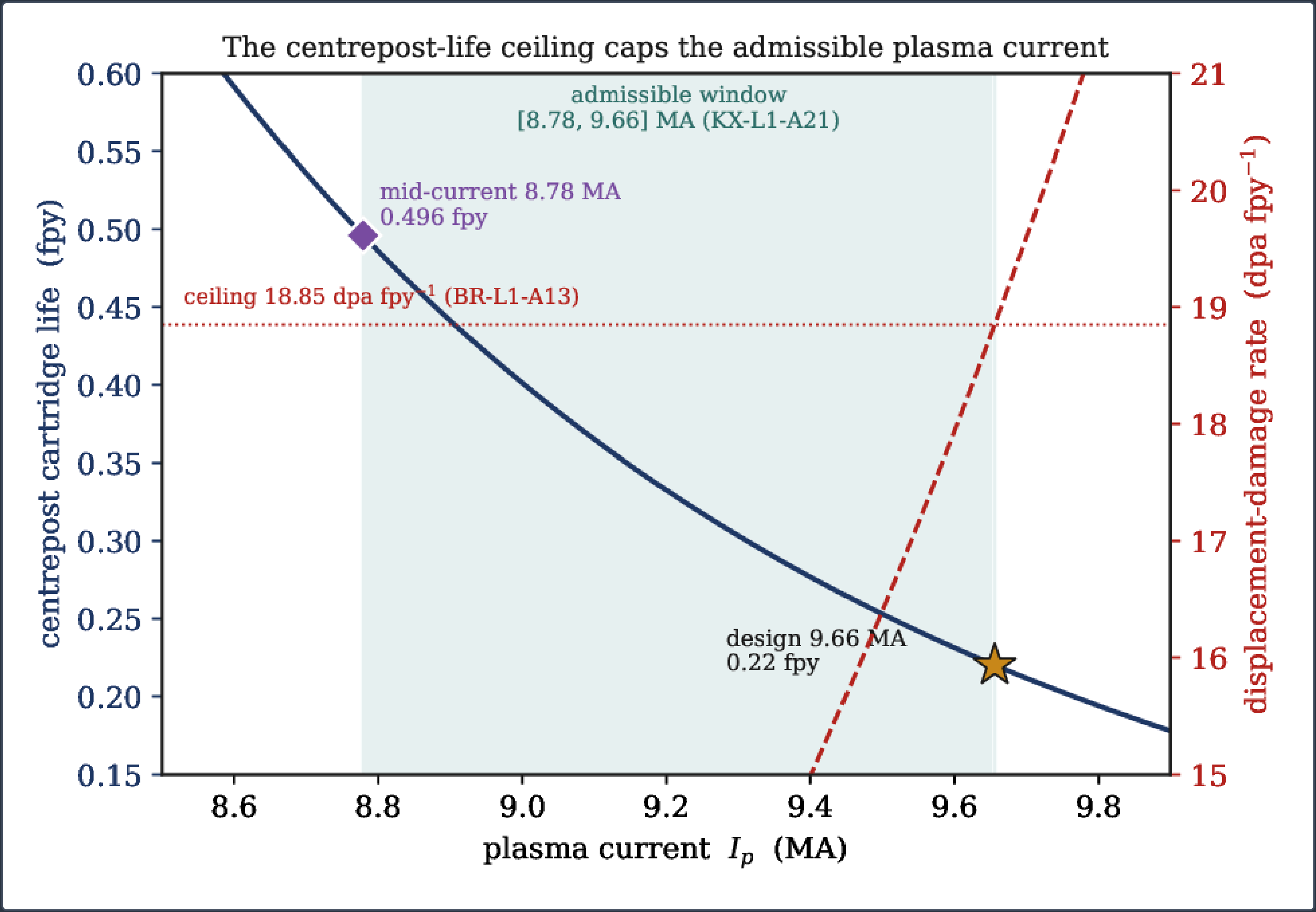

Cartridge life (navy, left) and displacement-damage rate (red, right) across the admissible plasma-current window [8.78, 9.66] MA (serial KX-L1-A21). The mid-current operating point extends life from 0.22 to 0.496 fpy; the dotted line is the 18.85 fpy^{-1} damage ceiling.

REPLACEMENT CADENCE AND FLEET AVAILABILITY

Equation (10) turns the design life directly into a replacement cadence: $n_{\text{swap}} = 1/0.22 \approx 4.5\,\text{swaps fpy}^{-1}$ at design (serial SC-BR-2; the 3-D CAD regression gives $4.9\,\text{swaps fpy}^{-1}$, serial BR-SX-12), falling to $\sim 2.0\,\text{swaps fpy}^{-1}$ at mid-current. Figure 8 pairs the cadence with the swap-limited fleet availability carried in the RAMI companions: 0.590 at design and 0.648 at mid-current (serials BR-SX-18, BR-SX-16), against a target capacity factor of 0.69. The swap cadence pulls availability below the target at both operating points — an honest negative — and the mid-current point is the recovery lever, trading source strength (and hence isotope throughput) for uptime. The per-swap outage critical path ($\sim 21.5\,\text{d}$, dominated $\sim 40\%$ by thermal cycling) and the ~ 39-swap thirty-year fleet history are analysed in the swap-logistics and fleet-availability companions [40,41]; the remaining-useful-life prognostics that schedule each swap are in the RUL companion [39].

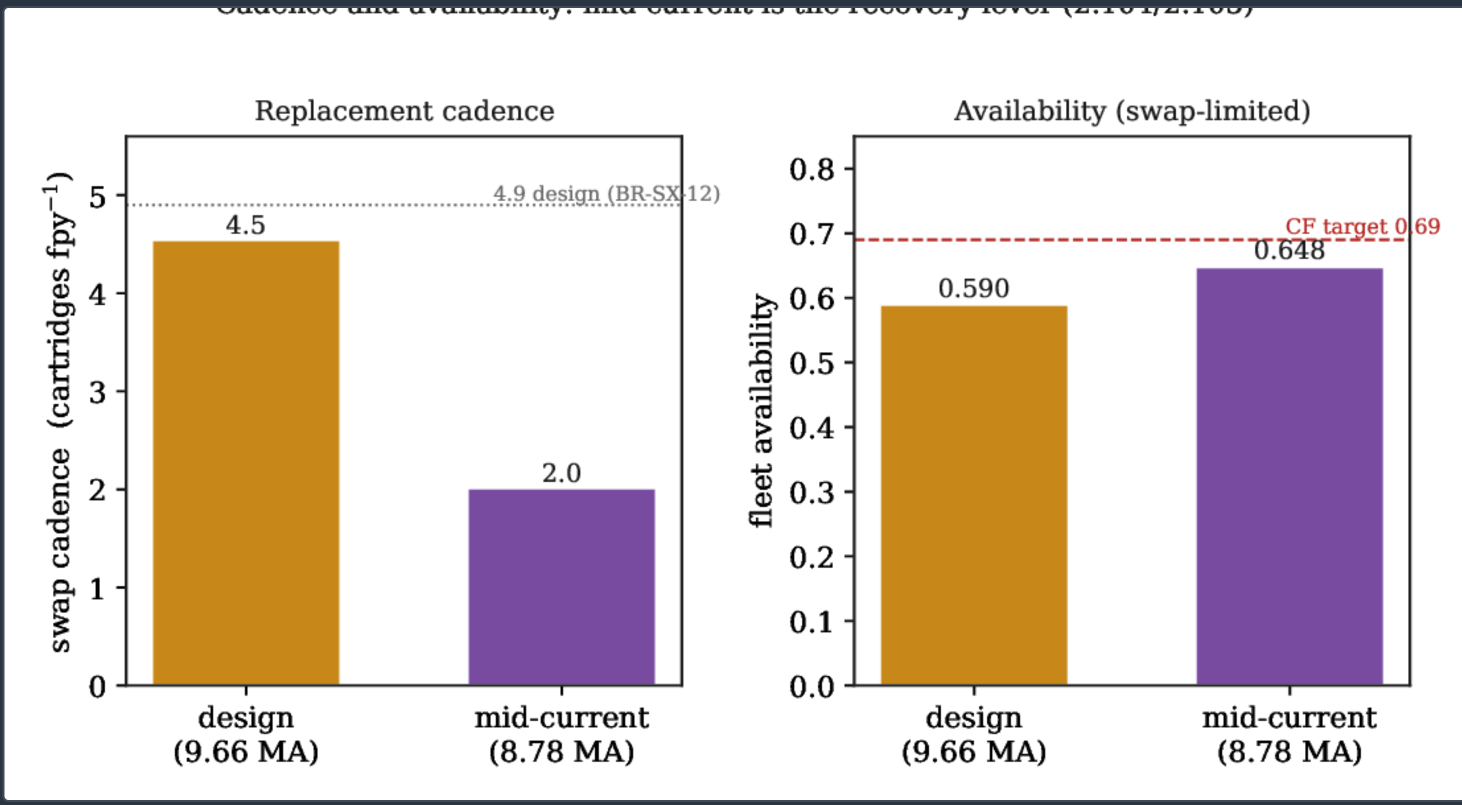

Cartridge replacement cadence (left) and swap-limited fleet availability (right) at the design and mid-current operating points (serials BR-SX-12, BR-SX-18, BR-SX-16). Availability is below the 0.69 capacity-factor target at both points; mid-current is the recovery lever.

DISPLACEMENT DAMAGE: NRT VERSUS ARC-DPA

Figure 9 shows the displacement function of equations (7)–(9): the NRT number grows linearly in damage energy, while the arc-dpa efficiency suppresses the surviving-defect count toward $\xi_{\mathrm{arc}} \to 0.3$ at the cascade energies ($\sim 15\,\mathrm{keV}$) resolved by the MD study of serial BR-L2-A24. The register anchors the design-basis damage rate on the conservative NRT convention (18.85 fpy^{-1}), so the arc-dpa reduction is carried as unclaimed margin rather than as a life extension; reporting the NRT number keeps the cartridge cadence on the safe side of the true surviving-damage rate.

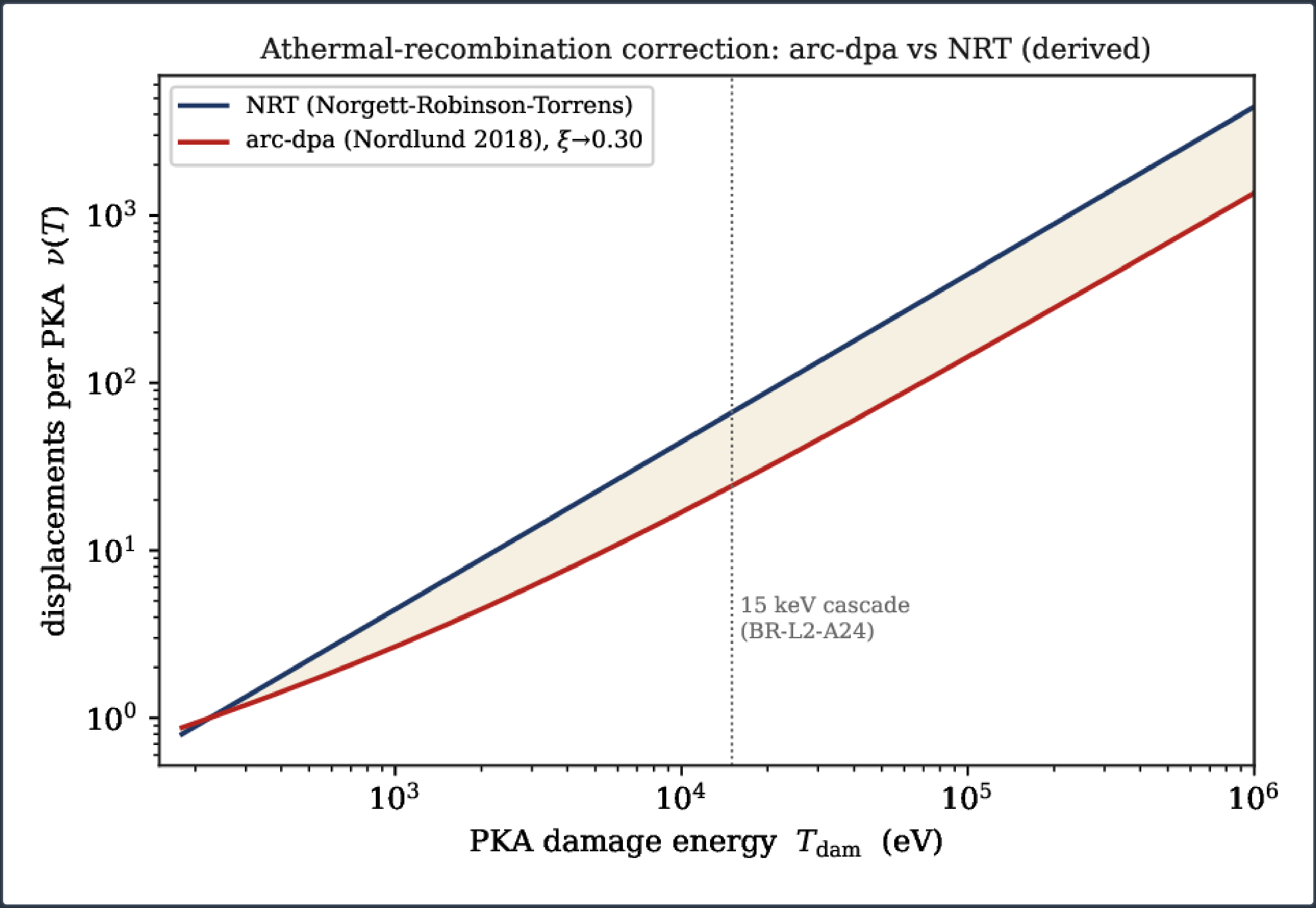

Displacements per PKA versus damage energy: NRT (equation 7) and the arc-dpa correction (equation 9, $\xi \to 0.30$). *(Derived model curve.)* The design-basis 18.85 fpy^{-1} is reported on the conservative NRT convention; the shaded region is unclaimed athermal-recombination margin.

§ 5

Discussion

AGAINST THE SHIELDED-SUPERCONDUCTING-CORE LITERATURE

The central finding — that a compact ST centrepost cannot be shielded to lifetime service within its inboard radius and is best operated as a consumable — agrees with, and quantifies, the shielded-core studies of Windsor *et al.*, who showed that even optimised tungsten- and tungsten-boride shields leave a superconducting centre column with a bounded, radius-limited protected life [7,8,9]. Our effective removal coefficient of $0.070 – 0.141\,/cm$ for WC and the factor-169 attenuation over $45\,cm$ are consistent with the order-of-magnitude-per-$\sim 20\,\mathrm{cm}$ attenuation those studies report for high-Z shields, and the depth-hardening of Σ_r^{eff} is the same buildup physics seen in point-kernel and discrete-ordinates shield calculations. The ARC demountable-magnet concept [3,4] motivates the cartridge architecture directly: once the magnet is demountable for maintenance, a scheduled fluence-limited swap is a design choice rather than a failure mode.

THE FLUENCE CEILING IN CONTEXT

The cartridge life depends linearly on the assumed REBCO fast-fluence ceiling, so the central number (0.22 fpy) is only as firm as Φ_{allow}. Our value [redacted] sits squarely inside the measured critical-current-degradation onset for coated conductors under fast-neutron irradiation reported by Fischer, Prokopec and Eisterer [19,20], and is set independently in the Kronos programme by first-principles DFT+U and cascade MD (companion [35]); the un-doped break-even fluence ([redacted]) and the $1 \times 10^{23}\,\mathrm{n\,m^{-2}}$ optimistic bound bracket a factor of ~ 2.6 in life. This is the dominant physics uncertainty on the cadence and is flagged as such.

DAMAGE CONVENTION AND STRUCTURAL LIFE

Reporting 18.85 fpy^{-1} on the NRT convention rather than ~ 5.7 fpy^{-1} on arc-dpa is a deliberate conservatism: the arc-dpa reduction (equation 9) is real, but folding it into the design rate would loosen the current window and the cadence, and we prefer the safe side. The first-wall and structural consequences of this damage rate — swelling, DBTT shift and helium embrittlement in the reduced-activation ferritic-martensitic steel and the tungsten first wall — are quantified in the companion first-wall studies [38,25,26] and are consistent with the fusion-materials limits [23,24].

BENCHMARK SYNTHESIS

Table 4 places the centrepost against the two reference points most often invoked for compact, high-field devices: the ARC-class demountable centre column and generic ST fusion-nuclear-science-facility inboard builds. The Kronos centrepost is on the same side of the trade — radius-limited protection, consumable operation — with the added, quantified constraint that the inboard shield is also in competition with breeding.

ATTRIBUTE	KRONOS CENTREPOST (THIS WORK)	COMPARABLE CONCEPTS
inboard-shield attenuation	$\times 169$ over 45 cm WC	~decade / 20 cm high-Z [8]
protected life	radius-limited, 0.22 fpy design	radius-limited (ARC-class) [3]
magnet strategy	demountable, scheduled cartridge	demountable magnets [3,4]
REBCO fluence ceiling	[redacted]	10^{22}–10^{23} measured [19,20]
distinguishing constraint	shield vs. inboard breeding	typically shield-only

Benchmark synthesis. The compact ST centrepost is fluence-limited and radius-limited in the same regime as comparable high-field / spherical concepts; the distinguishing constraint here is the shield-versus-breeding competition on a shared inboard radius.

§ 6

Limitations

One honest engineering gate remains open. The transport model is a 1-D radial infinite-cylinder CSG with reflective z-planes: it has no axial leakage, no divertor or port cutouts, and no toroidal-field ripple, and the triangularity $\delta = -0.30$ is not represented, so its net TBR is an upper-ish estimate for a given radial build and the true 3-D coverage is lower (recovered in the CAD-faithful companion). Separately, the "life" uses fast-fluence damage-limit proxies (equation 10), not a fully spectrum-folded NRT-dpa failure model of the conductor, so the absolute cadence scales inversely with the chosen Φ_{allow}. The single hard geometric gate is radial-budget closure: the centrepost winding plus a $30\,cm$ WC shield occupies $0.74\,m$, which overruns the available $R_0 - a = 0.72\,m$ inboard envelope by $\sim 2\,cm$ (serials BR-SX-13, BR-SXD-06). Structural ($181\,MPa$, $6\times$ margin) and quench budgets already pass; the $\sim 2\,\text{cm}$ overrun requires a shield/winding re-optimisation or a modest geometry relief and is carried as an explicit open item, not papered over.

§ 7

Conclusion

The inboard centrepost is the defining vulnerability of a compact spherical-tokamak breeder, and this paper quantifies it end-to-end. Solving the fixed-source Boltzmann transport equation on ENDF/B-VIII.0 with 2.5×10^9 histories per point, the centrepost fast fluence attenuates by a factor of 169 over a $45\,cm$ WC standoff, with an effective removal coefficient that hardens from 0.070 to $0.141\,/cm$ as buildup is stripped away. Folded against the REBCO fast-fluence ceiling [redacted], the design cartridge life is 0.22 fpy at a reference damage rate of 18.85 fpy^{-1}, tunable from 0.0048 (thin shield) to 0.194 fpy (thick shield) and extended to 0.496 fpy ($\times 2.25$) at the mid-current edge of the admissible current window $[8.78, 9.66]\,\mathrm{MA}$. The inboard shield trades directly against breeding (net 1-D TBR $1.035 \rightarrow 0.923$), and the coverage-versus-protection optimisation resolves — by an explicit KKT argument — to the corner design: give the full standoff to shield and recover self-sufficiency from the outboard blanket. The design consequence is a maintenance architecture, a demountable scheduled-swap cartridge at ~ 4.5–$4.9\,\mathrm{swaps\,fpy}^{-1}$ with a swap-limited availability of 0.59–0.65, stated as such rather than wished away. Every headline quantity is a frozen anchor in the de-risking register, and the one open gate — a $\sim 2\,\mathrm{cm}$ inboard radial-budget overrun — is named, not hidden.

Acknowledgments tocsectionAcknowledgments Part of the Kronos Fusion Energy 2026 design series. The authors thank the Kronos physics de-risking programme for the frozen result set underlying every quantitative claim, and R J Weggel and C Weggel for the centrepost magnet and radial-build engineering.

Reproducibility. Every headline quantity is a frozen anchor in the Kronos Physics De-Risking Register [33] (doi:10.5281/zenodo.22133057): the shield trade and fast-fluence attenuation (BR-L1-A13b), the reference damage rate (BR-L1-A13), the REBCO fast-fluence ceiling (BR-SX-04), the operating-point cartridge-life anchors (BR-SX-16, SC-BR-2) and the current window (KX-L1-A21). The OpenMC 0.15.3 model, the ENDF/B-VIII.0 inputs, the radial build and the figure-generation script are archived with this paper at doi:10.5281/zenodo.22645708; official version: https://www.kronosfusionenergy.com/publications/centrepost-fluence-and-shielding.html; no result depends on unpublished or proprietary data, and no economic quantity appears in the deposit.

Data availability tocsectionData availability The shield-trade tallies, the fast-fluence and net-TBR tables, the removal-coefficient and cartridge-life reductions and the figure scripts used for figures 3–9 are archived with the deposit at doi:10.5281/zenodo.22645708. All quantitative values trace to the register [33] by the serial identifiers cited inline.

Competing interests tocsectionCompeting interests Provisional patent applications relating to aspects of this work have been filed.

tocsectionReferences

APPARATUS

Portfolio, People & Record

The intellectual-property estate, the people who built it, the limitations that gate it, and the sources it rests on.

1	4	40	27
GRANTED PATENT	2026 PROVISIONALS	TEAM MEMBERS	2022 PROVISIONALS

INTELLECTUAL PROPERTY

The patent portfolio

The estate spans a granted high-field magnet patent, pending utility and 2026 provisional filings that map to the two products, a digital-twin control provisional, a registered trademark application, and the original 2022 provisional family. Every patentable disclosure in the five-paper arXiv drop was protected **before** publication: the breeder and burner provisionals were filed 1–2 August, and a publication-gap omnibus filing the evening before the drop swept up the DEC, plasma-control, and REBCO-winding matter of the three otherwise-unprotected papers. Patent numbers and application serials are matters of public record; claim scope is summarised, not reproduced.

GRANTED & PENDING UTILITY

US 12,009,112	High-field tilted graded-REBCO magnet architecture (KRONO-002A) · *app. 17/878,550*	GRANTED
US 17/878,507	Core device / method (KRONO-001A) · *utility*	PENDING

2026 PROVISIONAL FILINGS — MAPPED TO THE PRODUCTS

64/124,209	Hyperion — spherical-tokamak tritium / helium-3 foundry · *breeder · filed Aug 2026*	FILED
64/124,220	Aegis / MetroVolt — synchrotron-cutoff, fuel-selection & plug-winding · *generator · filed Aug 2026*	FILED
64/115,167	KRONOS-CTRL digital-twin plant control · *provisional · filed Jul 2026*	FILED
64/005,440	Integrated spherical-tokamak fusion architecture · *early integrated-architecture filing · filed Mar 2026*	FILED
64/105,530	Negative-triangularity spherical-tokamak architecture · *foundational ST filing · filed Jul 2026*	FILED
64/128,097	Publication-gap omnibus — quasineutral two-species expander DEC · provenance-gated / latency-split plasma control · as-built high-field winding & conductor architecture · *filed 7 Aug 2026, the evening before the arXiv drop*	FILED

TRADEMARK & ORIGIN

FTK-98801894	Kronos Fusion Energy — trademark application	FILED
KR-2022-*	Original provisional family (KR-2022-00001 … 00027) · *27 filings, 2022*	PRIORITY

The narrow, defensible magnet novelty — the specific conductor and the digital-twin winding optimisation, not high-field REBCO as a category — is the commercial core that can earn ahead of any Q > 1 milestone, with markets in fusion magnet supply, MRI/NMR, accelerators, and proton therapy. The claim is scoped honestly: the high field is a *system field* result, not a stand-alone-coil record; the small-bore plug coil is structurally infeasible as a bare winding but resolved by a stress-managed structural shield (feasible-pending-FEA); and the winding-tape experiment returned a *null result*. The value is the method, not a field record.

THE TEAM

Founding partners, board, advisors & auditors

Kronos is built by a bench of advanced-fuel-fusion, high-field-magnet, direct-conversion, and materials specialists, with a board and operations team drawn from defense, national laboratories, and industry. Dates are shown as ranges; where a tenure has ended or is term-ending, the range says so.

FOUNDING PARTNERS — SCIENCE

Dr. Gerald Kulcinski
Co-Founder · Helium-3 & Advanced-Fuel Fusion
UW–Madison · 2023–Present

Dr. Carl Weggel
Chief Scientist / S.M.A.R.T. Design
MIT Alcator Program · 2022–Present

Dr. Robert J. Weggel
Magnetic Field Design
MIT Magnet Lab · 2022–Present

BOARD

Priyanca Ford
Founder & CEO · Executive Board
2022–Present

Bandel Carano
Finance / Strategy
Oak Investment Partners / Stanford · 2025–2026

Patrick Schweiger
Fusion Device Engineering
Oklo / CFS / TerraPower · 2025–Present

SCIENTIFIC ADVISORS

Dr. Steven O. Dean
Fusion Policy & History
DOE / Fusion Power Associates · 2025–Present

Dr. Patrick H. Diamond
Plasma Turbulence & Transport
UC San Diego · 2025–Present

Dr. Jack J. Dongarra
HPC & Numerical Algorithms
Turing Award · 2025–Present

Dr. Nasr M. Ghoniem
Chief Material Scientist
UCLA · 2025–Present

Dr. Siegfried Glenzer
Plasma Physics & Laser Fusion
Stanford / SLAC · 2022–Present

Dr. David A. Hammer
Pulsed-Power Fusion
Cornell · 2025–Present

Dr. Donald A. Spong
Plasma Theory & Confinement
ORNL · 2025–Present

Dr. Curtis Smith
Risk Assessment & Nuclear PRA
MIT / Idaho National Lab · 2025–Present

RADM (Ret.) David Goggins
Naval Engineering & Power-Plant Design
U.S. Navy · 2023–2026

Dr. Konstantin Batygin
Mathematician
Caltech · 2022–2025

Dr. Ruben Fair
Magnet Design / ITER Liaison
PPPL / Jefferson Lab · 2022–2025

Dr. Paul S. Weiss
Materials & Nanotechnology
UCLA · 2022–2025

SCIENTIFIC AUDITORS

Dr. Wilfred A. Cooper
Plasma Equilibrium Theory
EPFL / Swiss Plasma Center · 2025–Present

Dr. Ahmed Hassanein
Plasma–Material Interactions
Purdue / Argonne · 2025–Present

Dr. Patrick E. Hopkins
Extreme Thermal Materials
U. of Virginia · 2025–Present

Dr. Peter Hosemann
Materials Joining & Structural Integrity
UC Berkeley · 2025–Present

Dr. Travis W. Knight
Advanced Nuclear Fuels & Systems
U. of South Carolina · 2025–Present

Dr. Philippe Lebrun
Cryogenics & Magnet Cooling
CERN · 2025–Present

Dr. Nitendra Singh
Nuclear Safety & Fuel Cycle
ITER · 2025–Present

Dr. Guido Van Oost
Magnetic Confinement & Fusion Systems
Ghent University · 2025–Present

Dr. Gary S. Was
Radiation Materials & Structural Integrity
U. of Michigan · 2025–Present

Dr. Ray Sedwick
Direct Energy Conversion
U. of Maryland · 2025

OPERATIONS

Michael Laughlin
Chief Operating Officer
2022–Present

Martin Owens
Chief Strategy Officer
LANL / GE Hitachi · 2022–Present

MG (Ret.) Paul Pardew
Chief Contracting Officer
Army Contracting Command · 2022–Present

David Beck
Fusion Commercialization
U.S. Space Force · 2024–Present

Sushma Bhatia
Environmental & Legislative
Google · 2022–Present

Michael De Frenza
Technology Licensing
2023–Present

MG (Ret.) Robin L. Fontes
Cybersecurity & Defense
Army Cyber Command · 2022–Present

Vijay Gehani
Supply Chain & Components
INOX India · 2024–Present

Jon Michel Greenwood
IT & AI Infrastructure
Live Nation · 2023–Present

Brian C. O'Neill
National Security
CIA / ODNI · 2022–Present

Gen. (Ret.) Gustave F. Perna
DoD Liaison
Operation Warp Speed · 2022–2023

Andrea Romero
Marketing Lead
2022–Present

Legal counsel is retained; those roles are held on the internal roster and are not listed here.

SOURCES

References

1 J E Menard *et al*, Fusion nuclear science facilities and pilot plants based on the spherical tokamak, *Nucl. Fusion* **56** 106023 (2016). doi:10.1088/0029-5515/56/10/106023

2 A E Costley, J Hugill and P F Buxton, On the power and size of tokamak fusion pilot plants and reactors, *Nucl. Fusion* **55** 033001 (2015).

3 B N Sorbom *et al*, ARC: a compact, high-field, fusion nuclear science facility and demonstration power plant with demountable magnets, *Fusion Eng. Des.* **100** 378 (2015). doi:10.1016/j.fusengdes.2015.07.008

4 A Q Kuang *et al*, Conceptual design study for heat exhaust management in the ARC fusion pilot plant, *Fusion Eng. Des.* **137** 221 (2018).

5 M Kovari *et al*, “PROCESS”: A systems code for fusion power plants — Part 1: Physics, *Fusion Eng. Des.* **89** 3054 (2014).

6 M Kovari *et al*, “PROCESS”: A systems code for fusion power plants — Part 2: Engineering, *Fusion Eng. Des.* **104** 9 (2016).

7 C G Windsor, J G Morgan and P F Buxton, Heat deposition into the superconducting central column of a spherical tokamak fusion plant, *Nucl. Fusion* **55** 023014 (2015).

8 C G Windsor and J G Morgan, Neutron and gamma flux distributions and their implications for radiation damage in the shielded superconducting core of a fusion power plant, *Nucl. Fusion* **57** 116032 (2017).

9 C G Windsor, J M Marshall, J G Morgan *et al*, Design of cemented tungsten carbide and boride-containing shields for a fusion power plant, *Nucl. Fusion* **58** 076014 (2018).

10 M J Norgett, M T Robinson and I M Torrens, A proposed method of calculating displacement dose rates, *Nucl. Eng. Des.* **33** 50 (1975).

11 G H Kinchin and R S Pease, The displacement of atoms in solids by radiation, *Rep. Prog. Phys.* **18** 1 (1955).

12 J Lindhard, V Nielsen, M Scharff and P V Thomsen, Integral equations governing radiation effects, *Mat. Fys. Medd. Dan. Vid. Selsk.* **33**(10) 1 (1963).

13 K Nordlund *et al*, Improving atomic displacement and replacement calculations with physically realistic damage models, *Nat. Commun.* **9** 1084 (2018).

14 K Nordlund *et al*, Primary radiation damage: A review of current understanding and models, *J. Nucl. Mater.* **512** 450 (2018).

15 A Yu Konobeyev, U Fischer, Yu A Korovin and S P Simakov, Evaluation of effective threshold displacement energies and other data required for the calculation of advanced atomic displacement cross-sections, *Nucl. Energy Technol.* **3** 169 (2017).

16 P K Romano, N E Horelik, B R Herman, A G Nelson, B Forget and K Smith, OpenMC: a state-of-the-art Monte Carlo code for research and development, *Ann. Nucl. Energy* **82** 90 (2015). doi:10.1016/j.anucene.2014.07.048

17 D A Brown *et al*, ENDF/B-VIII.0: The 8th major release of the nuclear reaction data library with CIELO-project cross sections, new standards and thermal scattering data, *Nucl. Data Sheets* **148** 1 (2018).

18 R E Macfarlane, D W Muir, R M Boicourt, A C Kahler and J L Conlin, The NJOY nuclear data processing system, version 2016, *Nucl. Data Sheets* **148** 189 (2018).

19 R Prokopec, D X Fischer, H W Weber and M Eisterer, Suitability of coated conductors for fusion magnets in view of their radiation response, *Supercond. Sci. Technol.* **28** 014005 (2015).

20 D X Fischer, R Prokopec, J Emhofer and M Eisterer, The effect of fast neutron irradiation on the superconducting properties of REBCO coated conductors with and without artificial pinning centers, *Supercond. Sci. Technol.* **31** 044006 (2018).

21 S Hahn *et al*, 45.5-tesla direct-current magnetic field generated with a high-temperature superconducting magnet, *Nature* **570** 496 (2019). doi:10.1038/s41586-019-1293-1

22 J L MacManus-Driscoll and S C Wimbush, Processing and application of high-temperature superconducting coated conductors, *Nat. Rev. Mater.* **6** 587 (2021). doi:10.1038/s41578-021-00290-3

23 S J Zinkle and G S Was, Materials challenges in nuclear energy, *Acta Mater.* **61** 735 (2013).

COLOPHON

How this document was made

The Kronos Fleet — Combined Editorial, 2026 is set in **Fraunces** (display), **Gelasio** (text), and **IBM Plex Mono** (data & equations), carried forward from the Kronos editorial design system.

The figures are rendered at 300 dpi from the deposited generator scripts; the document is composed as a single self-contained file with embedded fonts and imagery, paginated to US Letter, and rendered to PDF through a headless Chromium engine in matched light and dark editions.

Every headline quantity carries an evidence class; withdrawn and restated values are marked as such. Nothing herein is frozen beyond the founder-approved Tier-A set.

Explore it live — turn the interactive 3-D model, run the deposited solvers in the physics validator, and watch the companion film series.

LEGAL NOTICE

Notice, status, and distribution

Conceptual design & simulation study. This document reports a conceptual design and simulation study. It is not a construction commitment, a safety-analysis report, a regulatory filing, or an offer of securities. Forward-looking statements — schedules, costs, market sizes, and performance — are estimates subject to the limitations set out in the Simulations part and may change.

Numbers and their classes. Quantities are reported with evidence classes and case labels; modelled, assumed, and requirement-class values are identified as such and are not to be quoted without their labels.

Public edition. This edition carries the physics and design only; all financial, funding, and defense-commercial content has been removed for public distribution. The scientific text corresponds to the arXiv and journal submissions.

THE 2026 KRONOS SERIES

One programme, many papers

This editorial is one paper in the Kronos 2026 series — a real fusion company's complete, reproducible physics record for a spherical-tokamak breeder and its low-neutron D–^{3}He tandem-mirror burners. Every headline number is a frozen anchor in the Physics De-Risking Register.

Explore the whole programme: the De-Risking Register, the interactive 3-D model, and the physics validator.

KRONOS FUSION ENERGY

The Centrepost Life-Limiter: Fast-Fluence, dpa, and Shielding Setting the Cartridge-Replacement Cadence for a Compact Spherical-Tokamak Breeder

A real fusion company building real machines. Explore the science, live.

Zenodo · doi:10.5281/zenodo.22645708

Read on kronosfusionenergy.com

The Physics De-Risking Register